DOI: 10.1002/stco.202500026

Adrian Münch, Philipp Weidner, Thomas Ummenhofer, Valentin Larasser, Pauline Markreiter, Imke Engelhardt

ARTICLE

Experimental investigations of T-joints made of high-strength square hollow sections

This article presents experimental investigations on welded T-joints made of high-strength square hollow sections (S700MH and S890QH) under axial and bending loads, with and without preloading the chord. A total of 56 tests were conducted to analyse the influence of geometric parameters, material properties and pre-tensioning on joint behaviour and failure mechanism. The results are evaluated statistically and compared with current and draft Eurocode provisions (prEN 1993-1-8). The findings confirm that while the C_f-factor offers a conservative basis, refinements are necessary to account for distinct failure mechanism such as punching shear failure and the influence of loading direction, particularly for high-strength steels.

Keywords hollow section joints; high-strength steel; T-joint; experimental investigations; C_f-factor; static load-bearing behaviour

1 Introduction

1.1 Aim of the experimental studies of T-joints of rectangular hollow sections

Within the FOSTA research project P1504 [1], the static load-bearing behaviour of high-strength T-joints made of square hollow sections has been analysed. Currently, only limited experimental data exist for T-joints made of high-strength steels. In particular, the influence of chord preloading on the load-bearing capacity of such type of joints remains largely unexplored. For this reason, extensive experimental investigations have been carried out at the two research institutes, Research Center for Steel, Timber and Masonary of the Karlsruhe Institute of Technology (KIT) and the Institute for Material and Building Research of the University of Applied Sciences Munich, paying particular attention to the effect of chord preloading.

The experimental investigations provide the basis for gaining a better understanding of the load-bearing capacity and failure mechanism that occur in high-strength hollow section T-joints, especially due to the reduced deformation and load redistribution capacity of high-strength steels taking into account chord preloading and geometric parameters. In total, 56 static tests with varying parameters such as steel grade, β-ratio and chord preloading have been conducted. The statistical evaluation of the results of these tests allows to achieve a basis for a sound level of safety regarding a new proposal for the design of T-joints made of high-strength steels.

Besides the generation of data for a statistical evaluation, the tests with detailed strain measurements enable to verify numerical models to evaluate a wider range of geometric parameters. The respective numerical results are presented in [2].

2 State of the art

A statistical analysis of the available test data of tests on K-,N-,X- and T-joints [3–9] with yield strengths above 460 MPa shows that the wide scatter in the results can lead to conservative design values [1]. Furthermore, it can be shown that the mean value lines for chord face failure (CFF) and brace failure (BF) are close to values given by the design model provided in prEN 1993-1-8 [10]. Due to the small amount of data in some cases, the respective statistical uncertainty is high. In addition to the failure mechanism CFF and BF, there is a significant need to investigate punching shear failure (PSF). With the exception of the investigations shown in [7], the influence of chord preloading for high-strength steels has not been investigated so far experimentally in any configuration of T-joint. The strain fields resulting from the chord preloading lead to serious differences in the stress multi-axialities in the joint area of the braces compared to an unloaded chord. This issue must be critically assessed in the context of PSF and therefore requires targeted experimental investigation. The investigations of [11] already propose a yield point-dependent, linear chord pre-stressing function Q_y, which has already been numerically validated for CFF on the basis of tests on X-joints. For T-joints, however, the transfer of this Q_y-function has neither been verified numerically nor experimentally when considering the M–N interaction.

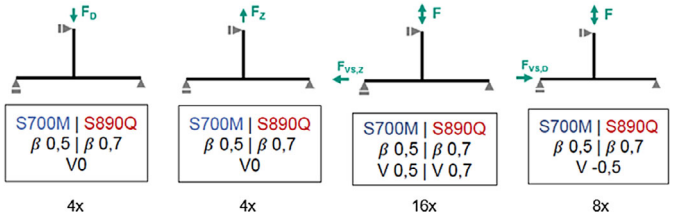

Fig. 1 Static system and loading direction depending on the degree of preloading [1]

To illustrate the test programme, the static system used for the axially loaded T-joint tests and the direction of loading of the brace and the chord are shown in Fig. 1 separately according to the degree of preloading.

Therefore, an urgent research demand exists, especially with respect to chord preloading effects in combination with brace bending or brace compression. This applies both to the extension of the database to include tests on steels with a yield strength of $f_y \approx 700$ N/mm^2 and to a steel grade of S890, which has not yet been provided for in prEN 1993-1-8 [10], taking into account the effect of chord preloading.

3 Test programme of the T-joint project

3.1 Test programme of T-joints under axial loading

The test programme for the ultimate load tests on axially loaded T-joints consists of 32 test specimens. The test specimens were manufactured from the high-strength steel grades S700MH and S890QH. This enabled an analysis of the influence of different manufacturing methods, cold-finished hollow sections according to DIN EN 10219-3 [12] and hot-finished hollow sections according to DIN EN 10210-3 [13], on the structural behaviour of high-strength hollow sections. The test programme distinguishes only four joint configurations made of the two steel grades mentioned above with two different β-ratios ($\beta = 0.5$ and $\beta = 0.7$) regarding geometric dimensions. Eight tests were carried out for each joint configuration. The degree of pre-stressing varies between a compressive preload ($n = -0.5$), no preload ($n = 0$) and tensile preload ($n = 0.5$ and $n = 0.7$). For each degree of preload, one test with axial tension and one test with axial compression of the brace are carried out. The nominal geometric dimensions as well as the dimensionless parameters of the four joint configurations are shown in Tab. 1.

3.2 Test programme of T-joints under bending

The test programme for the T-joints under bending loading covered 24 static tests. Therefore, the same four joint configurations were used as for the axially loaded T-joints (see Tab. 1). For each joint configuration, five different degrees of preload of the chord were tested as well as an additional buffer test. The test set up has been established to analyse the failure modes CFF and PSF.Fig. 2 shows the different loading conditions. A detailed description of the test concept is given in [14].

Tab. 1 Nominal geometric dimensions and dimensionless parameters of the four joint configurations

	Steel grade	Chord	Brace	2γ	β	τ
SHS	S700MH	100.0 × 5.0	50.0 × 3.0	20.0	0.50	0.60
	S890QH	100.0 × 5.6	50.0 × 5.6	17.9	0.50	1.00
	S700MH	100.0 × 5.0	70.0 × 3.0	20.0	0.70	0.60
	S890QH	100.0 × 5.6	70.0 × 5.6	17.9	0.70	1.00

4 Experimental investigations

4.1 Test setup

Fig. 3a shows the 3D CAD model of the test setup for the axially loaded T-joints with tensile preload. For a better overview, individual components such as the portal to which the test piston is attached are hidden. The axial force is applied to the T-joint by the aforementioned test piston. The supports, shown in Fig. 3a as bearings for the axial tensile load, enable the transfer of the load into the strong floor. The preload is applied to the chord as a tensile force by four pistons mounted horizontally on a tensioning block using tension rods with an adjustable length. The applied force is also short-circuited via the strong floor. The tests with pre-tensioned chords were always carried out in two load steps. In the first load step, the T-joint was pre-tensioned without any connection to the vertical test piston. After that, the resulting change in length was compensated by the turnbuckles of the tension rods, so that the T-joint can be coupled to the vertical test piston with the pre-tensioned chord without any constraint. The vertical force was then applied in the second load step. A further test setup was used for the axial tests with compression preload (see Fig. 3b). The load transfer and procedure during testing were equivalent to the described test setup with tensile pre-stressing. Fig. 4 shows a test specimen installed in the test rig during the ongoing static test.

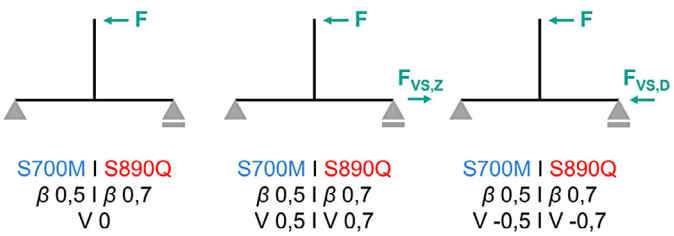

Fig. 2 Experimentally investigated loading conditions [1]

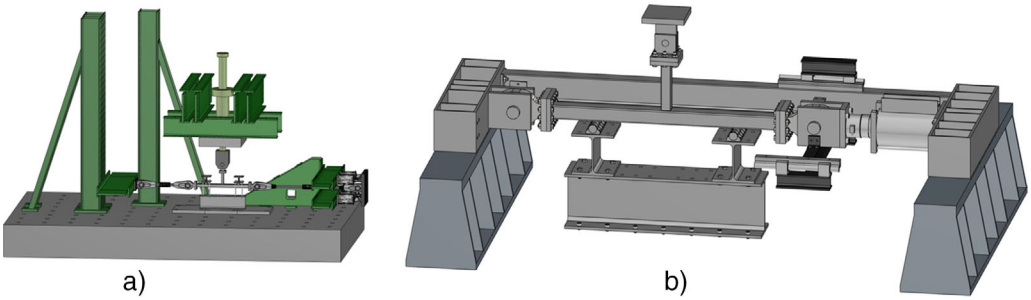

Fig. 3 Test setup for axially loaded T-Joints [1], a) for tension pre-load b) for compression pre-load

The test setup for the tests under brace bending has been already visualised in detail in [14]. The test rig consisted of a frame construction with two parallel frames and two pistons of different capacities with pre-slatted load cells. The piston for applying the load for the brace bending had a maximum tensile capacity of 400 kN and a maximum stroke of 250 mm. In order to avoid undesirable bending moments, a ball joint was also connected upstream of the load cell, which compensated for minor misalignments and thus ensured a constraint-free force application. A hydraulic cylinder with a nominal capacity of ±1600 kN (push and pull) and a maximum stroke of 400 mm was used to apply the chord preloading. The T-joint test specimens used in this test rig were connected to the frame and to the piston on all sides using swivel joints.

For the specimens without chord preload, only the 400 kN piston was required to apply the force to the brace in order to generate the bending moment under displacement control. The tests with chord preload were performed using a test programme under combined force and displacement control. The preload was applied and maintained in a force-controlled manner. Following that, the force was applied to the brace under displacement control. Due to the large chord deformation under compression loads, a maximum displacement of 1 mm under compression was specified as an additional termination criterion before switching to displacement control and keeping the displacement constant. This meant that any column buckling of the chord tube was avoided.

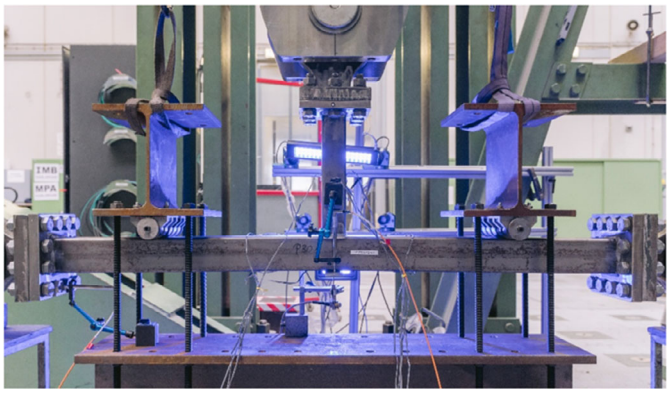

Fig. 4 Test specimen installed in the test rig [1]

4.2 Measurement technique

The T-joint tests are accompanied by measurement equipment to record all relevant parameters before and during the test. In addition to recording the force and displacement of each piston, supplementary measurement equipment such as displacement transducers (DTs), strain gauges and digital image correlation (DIC) systems were used in both research facilities in the area where high plastic strains are expected.

An important parameter for analysing the joint load-bearing capacity of T-joints is the percentage of indentation of the brace into the chord. A LIMESS DIC system was used to measure the indentation of the axially loaded T-joints. At the same time, the indentation was measured on the opposite side using a DT. Fig. 5 shows the comparison of the results given by the two measurement methods. The curves are superimposed and show that both measurement methods provide redundant measurement results. Basically, the indentation was analysed using the DIC measurements and the measurements with the DT served as a backup in case of a possible problem of the DIC system.

During the bending tests on T-joints, the local flange deformation of the SHS-T-joints was analysed using the GOM ARAMIS system. The aim was to record the local pull-out and the local indentation in a distance of 10 mm to the left (L10.LZ) and to the right (R10.LZ) of the brace and thus to determine the maximum values in the flange area of the chord around the brace. Fig. 6 shows the comparison of the moment–rotation relationship as well as the measured deformation.

5 Fabrication of specimens and material properties

5.1 Material and fabrication

In order to investigate high-strength steels with yield strengths $f_y > 700$ MPa, the project focused on the steel grades S700MH and S890QH when selecting materials whereas the profiles shall fulfil the requirements of

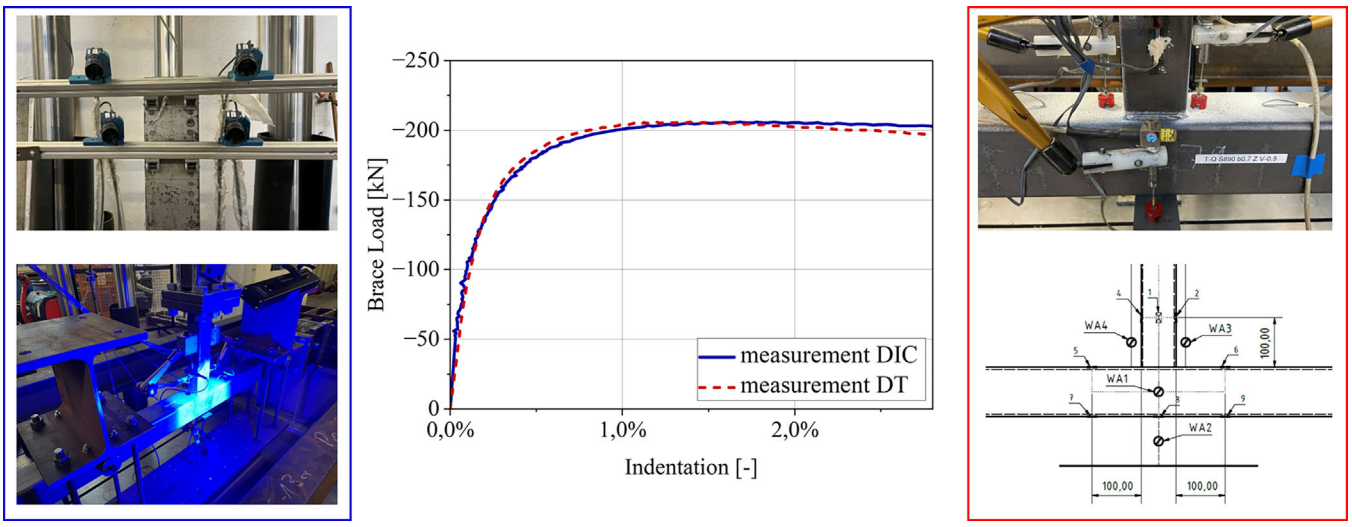

Fig. 5 Comparison of results given by the two measurement methods DIC and DT [1]

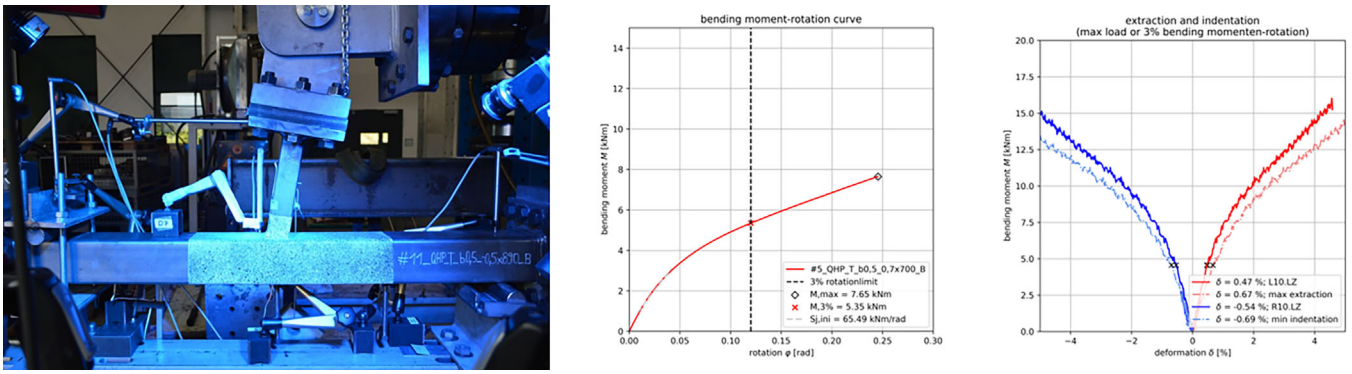

Fig. 6 Comparison of moment–rotation relationship and detected deformation measured by DIC [1]

cross-sectional class 1 or 2 according to Eurocode 3-1-1. Tab. 2 shows the nominal cross-sectional values and material characteristics taken from the factory certificates 3.1 according to DIN EN 10204 [15].

Welding tests were performed in order to develop qualified welding procedure specifications (WPS) for the production of the welds of the T-joints. As part of the tests, the filler material G89 6 M21 Mn4Ni2CrMo was selected in accordance with EN ISO 16834-A in order to achieve an even-matching ratio for the steel grade S890QH. To avoid softening or embrittlement of the high-strength material, the $t_{8,5}$ time was carefully specified and controlled. With a full penetration HV-seam containing the smallest possible z_0 dimension, it was intended to produce a butt weld (full connection). This ensured the maximal conservative influence on load-bearing capacity and stiffness of the joint, with respect to the geometry of the weld seam regarding load transfer, compared to thicker welds or combined fillet welds. Depending on the wall thickness of the brace, a single- or double-layer full penetration butt weld was necessary. According to the WPS, the weld start and stop

Tab. 2 Material characteristics of the hollow sections used to manufacture the test specimens

	Steel grade	Dimensions	Standard	R_{eH} [MPa]	R_m [MPa]	R_m/R_{eH} [–]	A5 [%]
SHS	S700MH	50 × 50 × 3.0	EN 10219-3	782	878	1.12	11.5
SHS	S700MH	70 × 70 × 3.0	EN 10219-3	794	875	1.10	10.5
SHS	S700MC	100 × 100 × 5.0	EN 10219-3	776	844	1.09	19.5
SHS	S890QLH	50 × 50 × 5.6	EN 10210-3	966	1048	1.08	18.5
SHS	S890QLH	70 × 70 × 5.6	EN 10210-3	964	995	1.03	17.9
SHS	S890QLH	100 × 100 × 5.6	EN 10210-3	976	1078	1.10	17.4

Tab. 3 WPS, S700MH/MC, single-layer butt weld without preheating (room temperature)

Weld bead	Welding position	Welding process	Filler material	Amperage	Voltage	Wire feed	Welding speed	Heat input
from–to	[–]	[–]	[mm]	[A]	[V]	[m/min]	[cm/min]	[kJ/cm]
1	PB	135	Ø 1.0	140–160	17–20	8.5–10	18–20	5.71–8.53
$t_{8,5}$ times from work samples: approx. **8–10 s** (root layer)								

Tab. 4 WPS, S890QLH, double-layer butt weld with preheating temperature of 60 °C and intermediate layer temperature of 70 °C

Weld bead	Welding position	Welding process	Filler material	Amperage	Voltage	Wire feed	Welding speed	Heat input
from–to	**[–]**	**[–]**	**[mm]**	**[A]**	**[V]**	**[m/min]**	**[cm/min]**	**[kJ/cm]**
1	PB	135	Ø 1.0	150	19	6.8	20–25	6.30
$t_{8,5}$ times from work samples: approx. **8–10 s** (root layer)								
2–3	PB	135	Ø 1.0	170	23.5	9.2	25–30	7.20
$t_{8,5}$ times from work samples: approx. **11–13 s** (top layer: 2-3)								

points had to be located in the unstressed flanks, as specified in DIN EN 1090-2, Annex E [16]. However, deferring from the WPS, welding was started by the manufacturer at the corner in an L-shape around the brace (no U-shape). The welding parameters are given in Tabs. 3 and 4.

5.2 Measurement of weld seam geometries

For the geometric evaluation of the weld seams, the seam angle, the a-dimension, the z_0-dimension, the z_1-dimension and the notch radius were determined at 16 measuring points on each T-joint (see Figs. 7, 8). With the help of a KEYENCE 2D laser profile sensor, the section profiles of the weld seams were recorded and analysed using laser triangulation measurements. The seam angles of the single-layer S700 samples have an average value of 45.2° and an a-value of $a = 3.84$ mm; the double-layer S890 samples have an average angle of 53.0 and an a-value of $a = 3.67$. The z_0-dimensions have an average value of $z_0 = 5.5$ mm (S700) as well as $z_0 = 4.63$ mm (S890) (Tab. 5).

Major differences result from the design of the single-layer seam of the S700MH-joints and the double-layer seam of the joints made of S890QLH. With an average z_0-dimension exceeding 4.6 mm, an influence of the supporting component of the width of the weld cannot be fully prevented.

6 Experimental results

6.1 Test evaluation

The load-bearing joint resistance of axially loaded T-joints is determined using the method described in [17, 18]. In principle, the joint resistance must be determined at the maximum of the force–indentation curve. However, the typical force–indentation curve of an axially loaded T-joint with a small β-ratio (see Fig. 10, blue line) shows that no maximum occurs. Due to the membrane forces, the brace is hooked into the upper flange of the chord and the load continued to increase with increasing deforma-

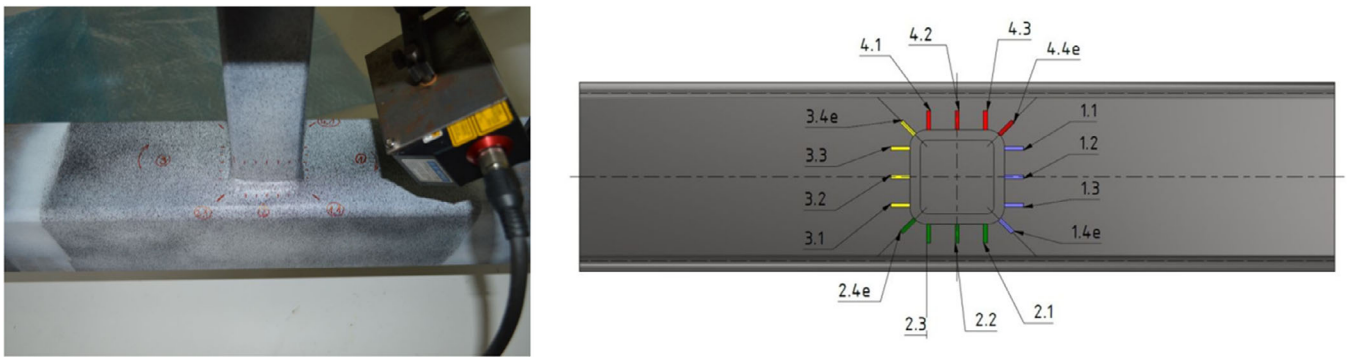

Fig. 7 Positions of the measured section profiles [1]

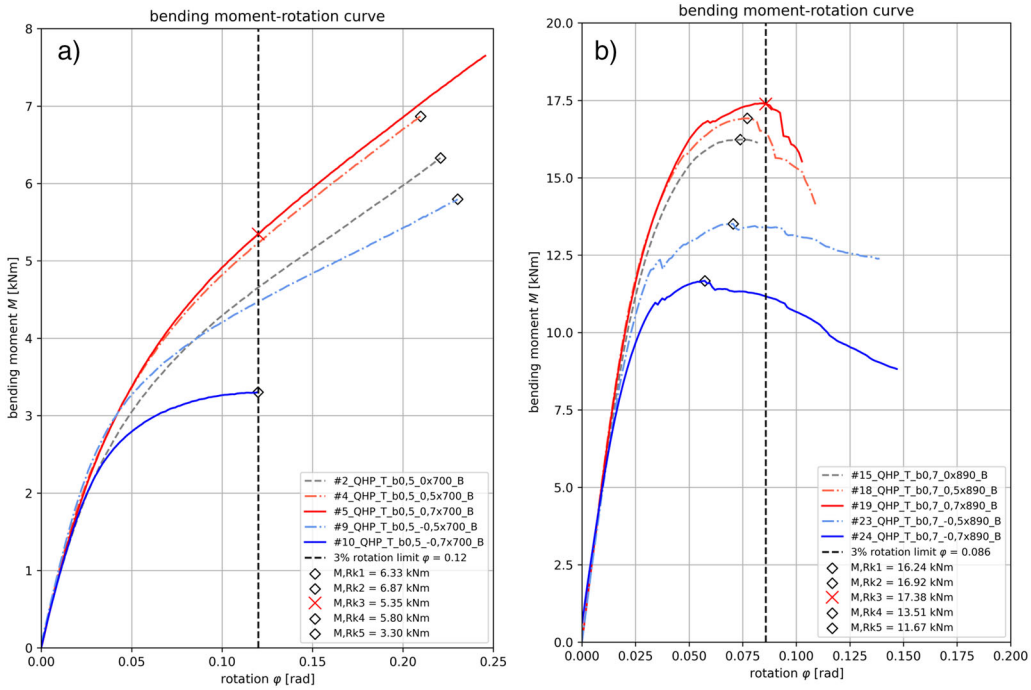

Fig. 8 Failure criteria for different experimentally derived moment–rotation curves [1] a) S700MH, b) S890QH

Tab. 5 Weld seam geometry, mean values of all test specimens (384 SW-seams)

Sample series Designation	Position No.	Seam angle [°]	a-dim [mm]	z_0-dim [mm]	z_1-dim [mm]	Notch radius [mm]	Quantity [−]
QHP-T-B_700	1.1-4.3_90°	47.80	3.82	5.23	5.75	1.28	144
QHP-T-B_700_e	1.4e-4.4e_90°	42.51	3.86	5.80	5.25	1.27	48
QHP-T-B_890	1.1-4.3_90°	53.60	3.69	4.56	5.86	0.99	144
QHP-T-B_890_e	1.4e-4.4e_90°	52.51	3.65	4.69	5.96	0.89	48

tion. For none of the tests with a small β-ratio carried out in the project P1504 [1], the load-bearing capacity could be reached. During the tests very large deformations occurred, see Fig. 10. In order to assess the load-bearing capacity of these joints, Lu et al. [17] developed the 3 % deformation criterion, which states that the load-bearing capacity of an axially loaded T-joint is reached at an indentation of 3% of the brace into the chord. The 3 % indentation was chosen by [17] because tests on T-joints with a higher β-ratio have shown that the maximum of the force–indentation curve of these tests is reached between an indentation of 2.5% and 5%. It has to be critically noted here that this evaluation of the tests compares a deformation criterion with the joint load-bearing capacity. Therefore, the method according to [17] is only used for compression loaded T-joints within this study. For those tests in which the brace of the T-joints was axially loaded in tension, a failure or a drop of load could always be

Fig. 9 Failure mechanisms depending on the type of loading [1]: a) no preload and compressive stress on the brace, b) no preload an tension stress on the brace, c) compression preload and tension stress on the brace

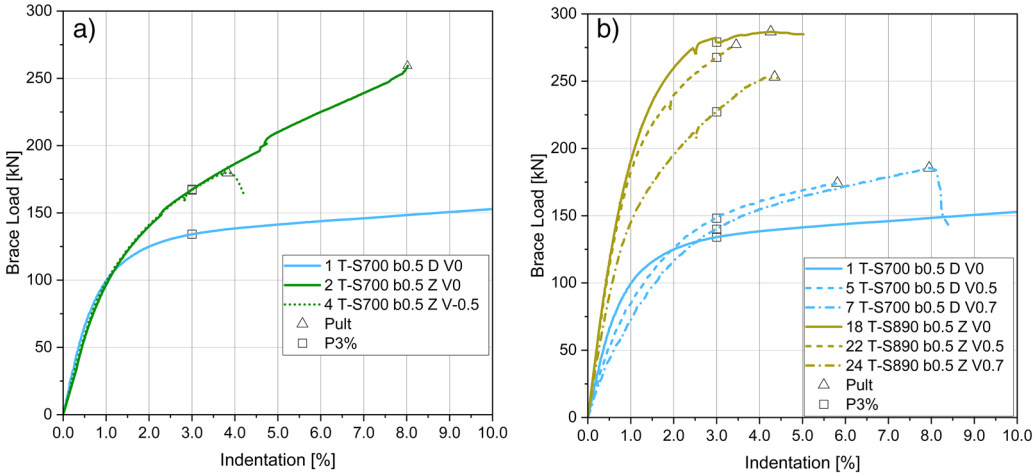

Fig. 10 Loadindentation curves: a) different failure mechanisms and b) influence of the tensile preload of the chord [1]

determined. For these tests the load-bearing capacity was determined at the ultimate load, regardless of whether the deformation criterion of 3% was exceeded or not. The same applies to all tests with high β-ratios.

A similar procedure has been applied for the evaluation of the bending tests. The load-bearing capacity was determined either by the maximum load, M_{max}, or by the intersection with the 3% deformation criterion. Following that, the minimum value was selected in the event that the maximum load was not reached initially. A subsequent comparison was made between the respective results and design values according to prEN 1993-1-8 [10]. The failure mechanism was classified based on the associated curves. Fig. 8 shows the different moment–rotation curves and Fig. 9 illustrates the corresponding failure mechanism.

For evaluation of the experimental results, a statistical analysis was carried out in accordance with DIN EN 1990:2021, Annex D [19]. This ensures that natural scattering in the material and geometric properties is adequately considered to guarantee the reliability and safety of provisions. The test results were compared with calculated resistances with respect to different failure mechanisms in accordance with prEN 1993-1-8 [10]. The design values were calculated without using the C_f coefficient, whereby the real strength and the real joint geometry parameters were used. By comparing these calculated load-bearing capacities with the experimentally determined maximum load-bearing capacities $r_e = N_{i.max}$, the mean value correction factor b was determined using a linear regression analysis.

6.2 Test results of axially loaded RHS-T-joints

Tab. 6 shows the joint load-bearing capacities calculated according to prEN 1993-1-8 [10] for the tests carried out with the associated governing failure mechanism under consideration of the measured dimensions of the respective test specimens. At this point it shall be noted that the design rules for determination of the joint load-bearing capacity in prEN 1993-1-8 for axially loaded T-joints do not distinguish with regard to the direction of loading of the brace. Therefore, the CFF is also decisive for T-joints subjected to axial tension. The joint load-bearing capacities in Tab. 6 differ only due to the difference in the respective geometric dimensions.

6.2.1 Load-deformation behaviour and failure mechanism: Axial loading

The test results of axially loaded T-joints made of high-strength steels show three failure mechanisms depending on the geometric parameters, the direction of preloading and the loading direction of the brace. The three observed failure mechanisms are shown in Fig. 9. Fig. 9a shows the typical failure mechanism CFF. In contrast, Fig. 9b shows the PSF mechanism that occurred in all tests in which the brace was subjected to an axial tension load. The joint load-bearing capacities of the T-joints subjected to axial tension are always higher than the joint load-bearing capacities of the same geometric configuration with the brace subjected to axial compression loading, regardless of the steel grade and the β-ratio (see Fig. 11). The third failure mechanism (Fig. 9c) shows a chord cross-section failure (CCSF). This failure mechanism is not covered by the standards yet but can be traced back to the performance of the tests. The tests were not carried out with a line bearing, so an M–N interaction also occurs in case of the axially loaded T-joints. The compressive preload is superimposed with the resulting bending moment causing a linear stress distribution, which supports a cross-section failure. The resulting bending moment can be reduced by selecting a smaller spacing of supports or by carrying out respective tests on X-joints. The tests that failed due to the failure mechanism shown in Fig. 9c or in which

Tab. 6 Comparison of joint load-bearing capacities and failure mechanisms according to prEN 1993-1-8 [10] and the test results

	Steel grade	Chord [mm x mm]	Brace [mm x mm]	LD[a)]	n_0	prEN [kN]	fm[b)]	Test [kN]	fm Test	n [−]
1	S700MH	100.0 × 5.0	50.0 × 3.0	C	0.0	107.3	CFF	134.1	CFF	1.25
2		100.0 × 5.0	50.0 × 3.0	T	0.0	110.9	CFF	167.4	PSF	1.51
3		100.0 × 5.0	50.0 × 3.0	C	−0.5	84.2	CFF	82.9	CFF	0.98
4		100.0 × 5.0	50.0 × 3.0	T	−0.5	82.2	CFF	166.9	CCSF[c)]	2.03
5		100.0 × 5.0	50.0 × 3.0	C	0.5	100.9	CFF	148.1	CFF	1.47
6		100.0 × 5.0	50.0 × 3.0	T	0.5	99.5	CFF	142.1	PSF	1.43
7		100.0 × 5.0	50.0 × 3.0	C	0.7	92.7	CFF	139.6	CFF	1.51
8		100.0 × 5.0	50.0 × 3.0	T	0.7	95.1	CFF	136.0	PSF	1.43
9	S700MH	100.0 × 5.0	70.0 × 3.0	C	0.0	163.9	CFF	206.1	CFF	1.26
10		100.0 × 5.0	70.0 × 3.0	T	0.0	165.9	CFF	279.4	PSF	1.68
11		100.0 × 5.0	70.0 × 3.0	C	−0.5	142.0	CFF	91.1	CCSF[c)]	0.64
12		100.0 × 5.0	70.0 × 3.0	T	−0.5	143.8	CFF	185.5	CCSF[c)]	1.29
13		100.0 × 5.0	70.0 × 3.0	C	0.5	158.5	CFF	249.8	CFF	1.58
14		100.0 × 5.0	70.0 × 3.0	T	0.5	154.5	CFF	210.1	PSF	1.36
15		100.0 × 5.0	70.0 × 3.0	C	0.7	148.8	CFF	251.6	CFF	1.69
16		100.0 × 5.0	70.0 × 3.0	T	0.7	147.0	CFF	–	PSF	0.00
17	S890QH	100.0 × 5.6	50.0 × 5.6	C	0.0	203.9	CFF	237.6	CFF	1.17
18		100.0 × 5.6	50.0 × 5.6	T	0.0	200.0	CFF	279.2	PSF	1.40
19		100.0 × 5.6	50.0 × 5.6	C	−0.5	157.3	CFF	160.6	CFF	1.02
20		100.0 × 5.6	50.0 × 5.6	T	−0.5	158.1	CFF	244.2	CCSF[c)]	1.54
21		100.0 × 5.6	50.0 × 5.6	C	0.5	204.5	CFF	258.1	CFF	1.26
22		100.0 × 5.6	50.0 × 5.6	T	0.5	206.4	CFF	267.5	PSF	1.30
23		100.0 × 5.6	50.0 × 5.6	C	0.7	205.0	CFF	266.5	CFF	1.30
24		100.0 × 5.6	50.0 × 5.6	T	0.7	152.7	CFF	227.0	PSF	1.49
25	S890QH	100.0 × 5.6	70.0 × 5.6	C	0.0	312.2	CFF	382.6	CFF	1.23
26		100.0 × 5.6	70.0 × 5.6	T	0.0	280.8	CFF	431.0	PSF	1.53
27		100.0 × 5.6	70.0 × 5.6	C	−0.5	256.7	CFF	192.9	CCSF[c)]	0.75
28		100.0 × 5.6	70.0 × 5.6	T	−0.5	276.8	CFF	272.4	CCSF[c)]	0.98
29		100.0 × 5.6	70.0 × 5.6	C	0.5	287.2	CFF	457.6	CFF	1.59
30		100.0 × 5.6	70.0 × 5.6	T	0.5	303.9	CFF	418.1	PSF	1.38
31		100.0 × 5.6	70.0 × 5.6	C	0.7	262.4	CFF	462.3	CFF	1.76
32		100.0 × 5.6	70.0 × 5.6	T	0.7	251.1	CFF	372.1	PSF	1.48

[a)] Loading direction of the brace (C: Compression, T: Tension);
[b)] failure mechanism;
[c)] chord cross-section failure

the plastic modulus of cross-sectional resistance of the chord was exceeded were not considered in the statistical analysis.

The three force–indentation curves of the tests shown in Fig. 10 show the expected deformation behaviour. As already described in Section 6.1, no failure was observed in the tests with a small β-ratio but large local deformations occurred. For these tests, the joint load-bearing capacity was determined according to the procedure given in [17]. T-joints that have been axially loaded in tension have a load-bearing capacity, but fail suddenly. The CCSF failure mechanism also occurs suddenly and results in a drop of load. Fig. 10b shows the influence of the tensile preload of the chord on the joint load-bearing capacity. For the T-joints subjected to axial compression, the pre-tensioning increases the joint load-bearing capacity, while for the T-joints subjected to axial tension, the pre-tensioning reduces the load-bearing capacity. Since prEN 1993-1-8 [10] does not differentiate between the loading direction of the brace but provides a reduction for both directions of preloading, this procedure is conservative.

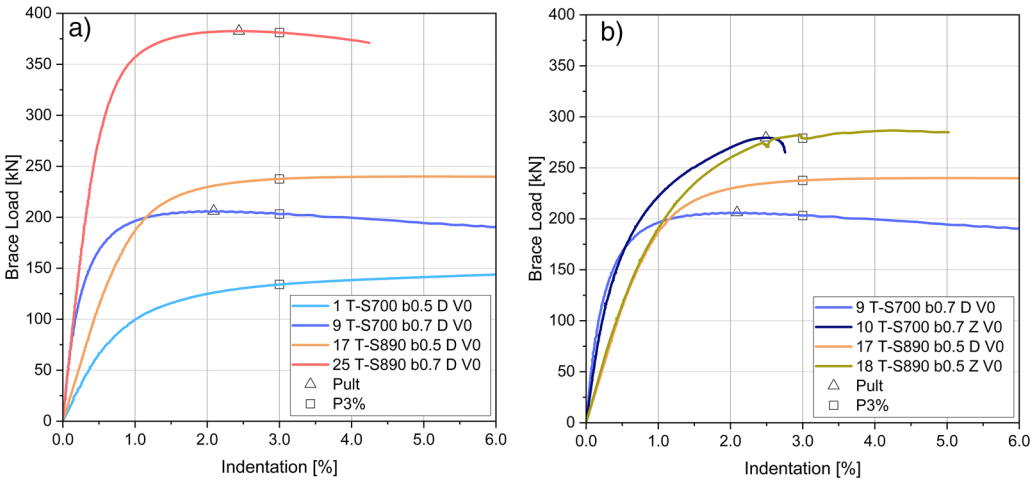

Fig. 11 Load–indentation curves: a) influence of the ß-ratio and b) influence of the loading direction of the brace [1]

However, a more efficient design would be possible if the loading direction of the brace is considered.

Fig. 11a illustrates the influence of the β-ratio. The tests with a β-ratio of $\beta = 0.7$ show a maximum, whereas the tests with a small β-ratio ($\beta = 0.5$) do not show a maximum and were cancelled due to the large deformations that occurred. The force–indentation curves in Fig. 11 also show that the β-ratio has a significant influence on the initial stiffness and joint load-bearing capacity.

6.2.2 Statistical evaluation – Axial loading

Fig. 12 shows the statistical evaluation of the T-joints subjected to axial compression in accordance with DIN EN 1990 Annex D [19]. Fig. 12a shows the statistical analysis of the results of the tests without pre-stressing and Fig. 12b shows the statistically analysed results of the joints with tensile pre-stressing. Both figures of the statistical evaluation show a characteristic statistical coefficient exceeding a value of 0.8. Since the joint load-bearing capacities r_t were calculated according to prEN 1993-1-8 without applying a C_f-factor, the statistical coefficient can be directly interpreted as the C_f-factor. The results thus show that the design rules for determining the joint load-bearing capacities according to prEN 1993-1-8 are on the safe side. The statistical evaluation of the tests with tensile pre-stressing shown in Fig. 12b shows a significantly higher coefficient of variation ($V_\delta = 0.118$). The coefficient of variation and thus the large scatter indicate that the chord stress function Q_f of the design formulae according to prEN 1993-1-8 [10] does not adequately reflect the influence of the tensile pre-stressing. This result can also be derived from the force–indentation curves, which show that a pre-tensioning of the chord increases the joint load-bearing capacity of a brace subjected to axial compression (see Fig. 10). In contrast, the chord stress function Q_f according to prEN 1993-1-8 [10] always results in a

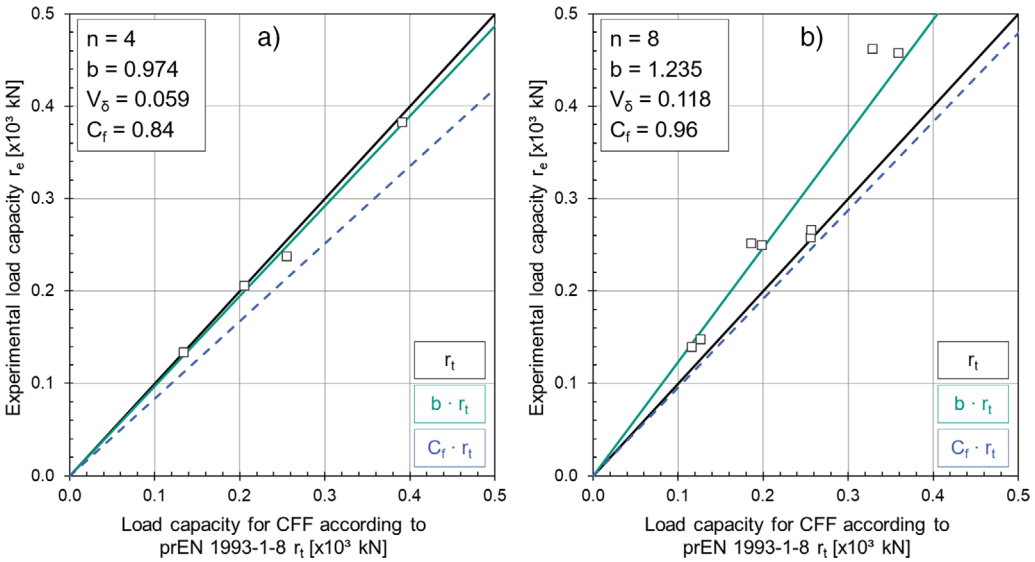

Fig. 12 Statistical evaluation of T-joints subjected to axial compression (CFF) [1] in accordance with DIN EN 1990 Annex D [19]

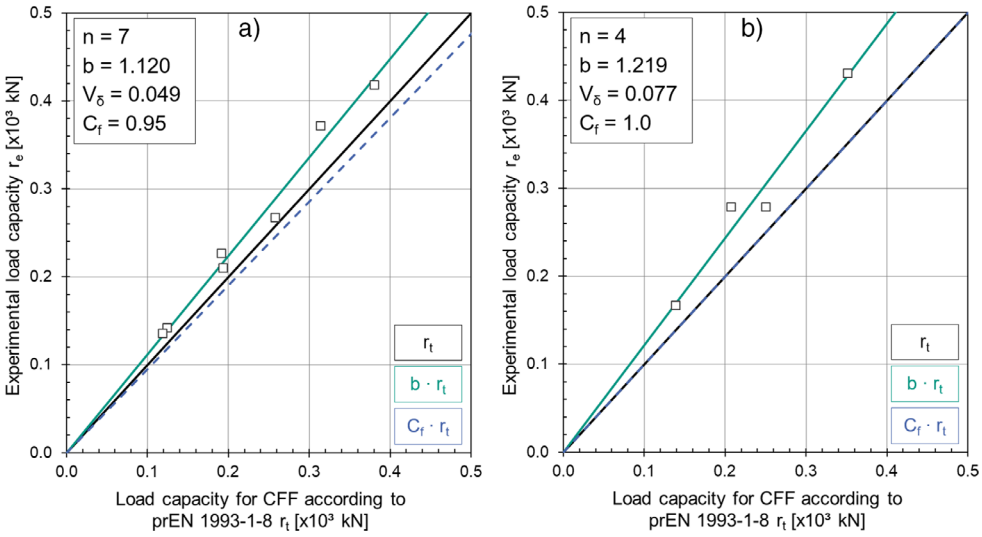

Fig. 13 Statistical evaluation according to DIN EN 1990 Annex D [19] of T-joints subjected to axial tension (CFF) [1]

decrease in joint load-bearing capacity. The same statistical analysis was also carried out for T-joints subjected to axial tension (see Fig. 13). It can be seen in Fig. 13b that the chord stress function Q_f provides a good estimation for a brace subjected to tension ($V_\delta = 0.049$), as the tensile pre-stressing of the chord reduces the joint load-bearing capacity in the tests. In this evaluation, however, the tests with a PSF are compared with the resistance model for chord face plastification, as this failure mechanism is decisive according to [10].

When comparing the experimental results with the PSF predictions, it becomes apparent that the model given in [10] consistently overestimates the joint load-bearing capacities, leading to a non-conservative and inaccurate representation of the observed behaviour (see Fig. 14). In addition, the chord stress function Q_f is not included in the design formulae for PSF, but the tests also show an influence of the chord pre-stressing for PSF.

6.3 Test results of RHS-T-joints under bending loading

Tab. 7 presents the joint load-bearing capacities calculated in accordance with prEN 1993-1-8 [10], assuming a C_f-factor of $C_f = 1.0$. For PSF, a factor of $1.0 \cdot f_y$ was applied instead of the conventional $0.8 \cdot f_u$. The results correspond to the measured specimen dimensions and material properties, with failure mechanism assigned based on the governing failure mechanism observed in each test.

6.3.1 Load-deformation behaviour and failure mechanism: Bending

The analysis of local deformation behaviour reveals a complex interaction between brace rotation and localised plastic deformation in the chord. Depending on the chord preloading, different local pull-outs and indentations

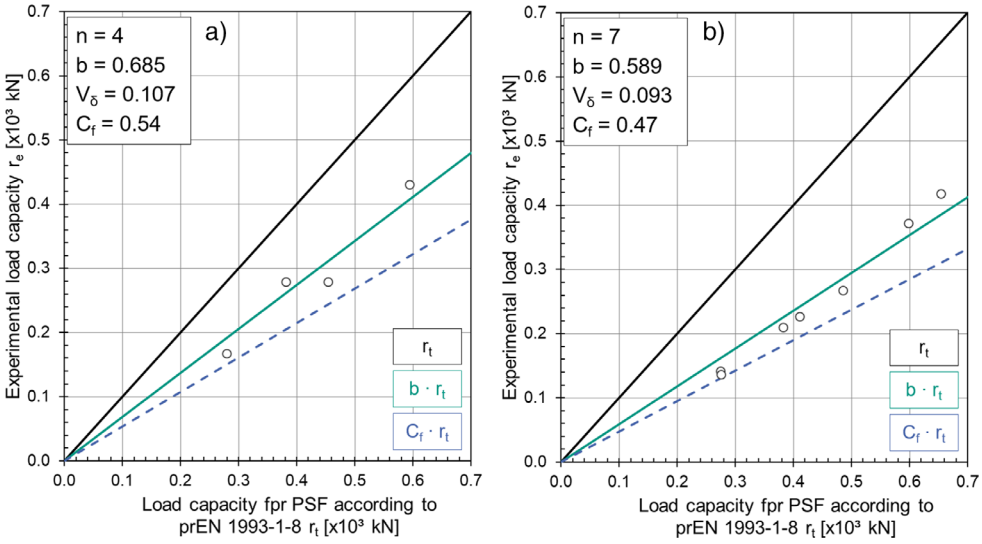

Fig. 14 Statistical evaluation in accordance with DIN EN 1990 Annex D [19] of T-joints subjected to axial tension (PSF) [1]

Tab. 7 Comparison of joint load-bearing capacities and failure mechanisms according to prEN 1993-1-8 [10] and the test results

	Steel grade	Chord [mm × mm]	Brace [mm × mm]	LD[1)]	n_0	M_{Rk} prEN [kNm]	fm[2)]	M_e test [kN]	fm test	n [–]
1	S700MH	100.0 × 5.0	50.0 × 3.0	B	0.0	4.32	CFF	4.63	CFF	1.07
2		100.0 × 5.0	50.0 × 3.0	B	0.5	4.12	CFF	5.26	CFF	1.28
3		100.0 × 5.0	50.0 × 3.0	B	0.7	3.77	CFF	5.40	CFF	1.43
4		100.0 × 5.0	50.0 × 3.0	B	−0.5	3.32	CFF	4.43	CCF	1.34
5		100.0 × 5.0	50.0 × 3.0	B	−0.7	3.29	CFF	3.25	CFF	1.16
6	S700MH	100.0 × 5.0	70.0 × 3.0	B	0.0	8.71	CFF	10.08	CFF	1.16
7		100.0 × 5.0	70.0 × 3.0	B	0.5	7.95	CFF	9.65	CFF	1.21
8		100.0 × 5.0	70.0 × 3.0	B	0.7	7.61	CFF	10.30	CFF[)]	1.35
9		100.0 × 5.0	70.0 × 3.0	B	−0.5	6.95	CFF	8.49	CFF[)]	1.22
10		100.0 × 5.0	70.0 × 3.0	B	−0.7	5.97	CFF	5.6	CFF	0.94
11		100.0 × 5.0	70.0 × 3.0	B	−0.7	5.94	CFF	6.50	CFF	1.09
12	S890QH	100.0 × 5.6	50.0 × 5.6	B	0.0	7.64	PSF	9.45	CFF	1.24
13		100.0 × 5.6	50.0 × 5.6	B	0.5	7.75	PSF	8.82	PSF	1.14
14		100.0 × 5.6	50.0 × 5.6	B	0.7	7.27	CFF	8.82	PSF	1.12
15		100.0 × 5.6	50.0 × 5.6	B	−0.5	6.50	CFF	6.74	CCF	1.04
16		100.0 × 5.6	50.0 × 5.6	B	−0.7	5.45	CFF	6.23	CFF	1.14
25	S890QH	100.0 × 5.6	70.0 × 5.6	B	0.0	15.42	PSF	16.24	PSF	1,05
26		100.0 × 5.6	70.0 × 5.6	B	0.5	15.66	CFF	16.92	PSF	1.08
27		100.0 × 5.6	70.0 × 5.6	B	0.7	14.74	CFF	17.40	PSF	1.18
28		100.0 × 5.6	70.0 × 5.6	B	−0.5	13.72	CFF	13.51	CFF	0.98
29		100.0 × 5.6	70.0 × 5.6	B	−0.7	11.29	CFF	12.25	CFF	1.08
30		100.0 × 5.6	70.0 × 5.6	B	−0.7	11.70	CFF	11.67	CFF	0.98

occurred for the same steel grade and specimen geometry. These results indicate a multiaxial stress-related deformation of the flange in the immediate vicinity of the brace. Moreover, indentation deformations generally exceeded pull-out deformations in magnitude. Due to the increasing tensile force in the chord with rising brace load, the occurrence of pull-out deformations appears not intuitive. However, the local deformation measurements indicate that a calculated brace rotation of 3% corresponds approximately to a proportional deformation with either pull-out or indentation of 3% in the adjacent chord flange area. On average, the maximum deflection at a brace rotation of 3% is –2.822%, while for the pull-out a value of 2.541% is observed.

The failure mechanism was determined by the local rotation behaviour because failure mechanism often occurs in combination. Exceeding the 3% criterion before a noticeable drop indicates CFF, while a drop before reaching this criterion indicates PSF.

The major failure mechanism received was CFF for the T-joints made of S700 and S890 under bending loading. PSF only occurred for the T-joints made of S890 without chord pre-stressing as anticipated by prEN 1993-1-8:2021 [10] and in specimens with tensile preloading. However, in the latter case, the current design code prEN 1993-1-8:2021 [10] still identifies CFF as the governing failure mechanism. This highlights that the current design provisions do not always accurately capture the failure mechanism of hollow section joints made of high-strength steels.

6.3.2 Statistical evaluation – Bending loading

Fig. 15 shows the statistical evaluation of the bending tests considering the real yield strength of the material for the calculated load-bearing capacities. For the 11 test specimens made of steel grade S700MH, the C_f-factor is $C_f = 0.92$ and for the specimens made of S890QLH it is $C_f = 0.90$. Even when using the yield strength f_y rather than $0.8 \cdot f_u$ for the PSF failure mechanism, the resulting C_f-factor remained above the normative C_f-factor of $C_f = 0.80$ in prEN1993-1-8 [10], indicating inherent safety in the current formulation.

Analysing the S700MH data shows significant differences for the C_f-factor under compressive and tensile loads. For the five specimens with compressive chord pre-stressing, the resulting C_f-factor is 0.89, slightly above the safety

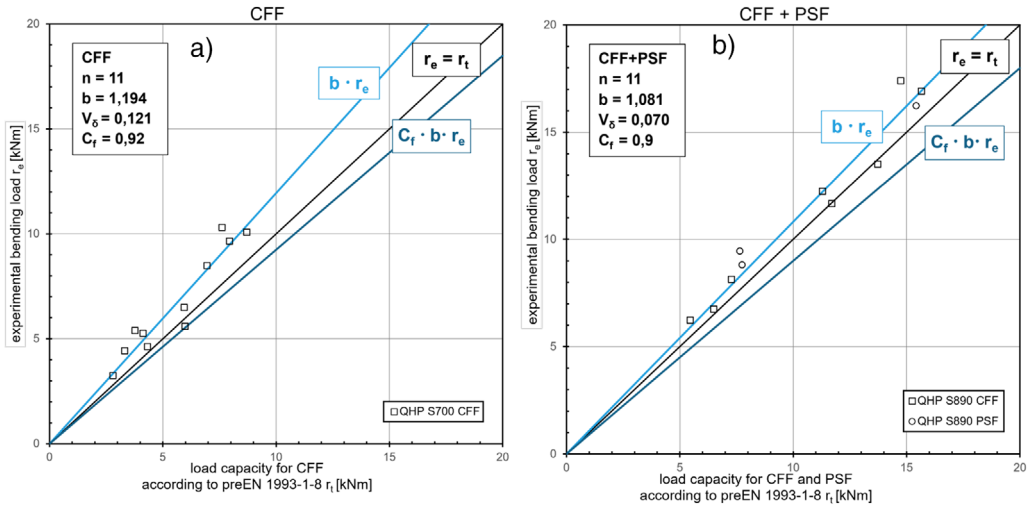

Fig. 15 Statistical evaluation in accordance with DIN EN 1990 Annex D [19] of T-joints subjected to bending loading by steel grade: a) S700MH and b) S890QLH [1]

threshold of 0.80. The tests with four test specimens under chord tension result in a C_f-factor of 1.07 so that chord preload under tension leads to an increased load-bearing capacity compared to a chord with no preload or compressive preload. The eight specimens made of S890QLH with CFF show a C_f-factor of 0.90, which is above the safety threshold of 0.80. A b-value of 1.076 is obtained, with a corresponding variance of 0.064, indicating a relatively low scatter in data. This indicates a high level of consistency in the measurement data. The three test specimens that exhibit PSF perform similarly consistently. With a C_f-factor of $C_f = 0.89$, the safety level is still above the required value of $C_f = 0.80$ according to prEN 1993-1-8:2021 [10]. The variance of 0.080 remains within an acceptable range and does not indicate irregularities in the test results. Even for this abrupt failure mechanism, the regression line value of 1.098 exceeds the characteristic standard value by 9.8%.

Tab. 8 shows the complete statistical evaluation of the C_f-factors based on the use of either f_y or $0.8 \cdot f_u$ for the calculation of PSF. The aim of this investigation was to check whether the additional reduction of $0.8 \cdot f_u$ can be omitted and to evaluate the potential for adapting the existing design provisions accordingly. However, only 7 of the 20 test specimens exhibited PSF, meaning that the C_f-factor was primarily influenced by the S890QLH specimens showing this failure mode. Substituting $0.8 \cdot f_u$ with f_y did not lead at a significant reduction in the resulting C_f-factors.

Tab. 8 Cf-factors for SHS-T-joints, bending loading

Steel grade (number of tests) Total number 22 incl. buffer tests[a)]	**C_f-factor with f_y**	**C_f-factor with $0.8 \cdot f_u$**
S700MH ($n = 11$)	0.92	0.96
S890QLH ($n = 11$)	0.90	0.90
S700MH FM CFF ($n = 11$)	0.92	0.96
S700MH PS C ($n = 5$)	0.89	0.89
S700MH FM T ($n = 4$)	1.07	1.14
S890MH FM CFF ($n = 8$)	0.90	0.86
S890MH FM PSF ($n = 3$)	0.89	1.04
S890MH PS C ($n = 5$)	0.86	0.86
S890MH PS T ($n = 3$)	0.96	1.07

[a)] FM, failure mode; PS, pre-stressing; C, compression; T, tension

7 Conclusion

In summary, the test results of the axially loaded T-joints made of high-strength steels demonstrate that that the loading direction of the brace must be considered as it leads to distinct failure mechanism, each requiring assessment based on its specific failure model. In particular, the PSF model should be revised according to the test results including the influence of chord pre-stressing, which proved to be a significant parameter. Furthermore, the design models in prEN 1993-1-8 [10], which are calibrated on normal-strength steels, cannot be directly applied to high-strength steel joints. Material-specific adjustment factors are required to account for the specific properties of high-strength steels. According to the test results, the C_f-factor introduced in the current draft of prEN 1993-1-8 [10] was found to be conservative across all evaluated configurations. However, to validate its general applicability, further numerical studies for an extended parameter range are required.

Overall, the bending loaded T-joints of fine-grained steel S890QLH exhibit reliable joint load-bearing capacity with low scatter in data. The S700MH specimens with tensile chord pre-stressing showed particular high load-bearing and rotational capacities. The

theoretical load-bearing capacities according to prEN 1993-1-8 [10] were initially confirmed as conservative for all configurations. Across all test series, the C_f-factor remained at or above 0.9 and thus exceeding the conservative reference value of $C_f = 0.8$ defined in [10]. This also applies to T-joints assessed for punching shear, even when the yield strength f_y is used instead of $0.8 \cdot f_u$. Chord tension and chord compression pre-stressing have different effects on the load-bearing capacity. A chord tension pre-stressing leads to a higher load-bearing capacity, while a compression pre-stressing leads to a slight reduction of the load-bearing capacity compared to an unloaded chord, resp. a preload equal to zero. It must also be acknowledged that the failure modes predicted in prEN 1993-1-8 [10] do not always align with those observed experimentally.

In summary, the C_f-factor currently specified in prEN 1993-1-8 [10] can be considered conservative and robust. For the failure mode PSF, the use of the full yield strength f_y in design instead of using $0.8 \cdot f_u$ appears justifiable based on the test data.

Acknowledgements

The research project 'Static load-bearing behaviour of high-strength T-joints made of rectangular hollow sections under consideration of the chord preloading influence in steel construction, FOSTA research project P1504' was funded by the Federal Ministry of Economic Affairs and Climate Action as part of the 'Industrial Collective Research' programme based on a resolution of the German Bundestag. This project IGF-Nr. 01IF21437N / P1504 from the Research Association for steel Application (FOSTA), Düsseldorf, was carried out at Karlsruhe Institute of Technology (KIT) and at the University of Applied Sciences Munich University of Applied Sciences Munich. The authors are grateful to the Research Association for Steel Application (FOSTA) for their financial support as well as all the industry partners for supplying materials and performing the welding work.

Open access funding enabled and organized by Projekt DEAL.

References

[1] Ummenhofer, T.; Engelhardt, I.; Münch, A.; Weidner, P. (2024) *Static load-bearing behaviour of high-strength T-joints made of rectangular hollow sections under consideration of the chord preloading influence in steel construction, FOSTA research project P1504*. Düsseldorf: Forschungsvereinigung Stahlanwendung e.V. (FOSTA).

[2] Markreiter, P.; Münch, A.; Engelhardt, I.; Weidner, P. (2025) Numerical investigations of T-joints made of high strength square hollow sections. Steel Construction 18, No. 3, pp. 194–208. https://doi.org/10.1002/stco.202500025

[3] Mang, F.; Bucak, Ö.; Steidl, G. (1982) *Untersuchungen an Verbindungen von offenen und geschlossenen Profilen aus hochfesten Stählen. Projekt 11*. Stud. Für Anwendungstechnik Von Eisen Stahl EV Düsseld., Dec.

[4] Liu, D. K.; Wardenier, J. (2004) *Effect of the yield strength on the static strength of uniplanar K-joints in RHS*. Doc IIW-XVE-04-29.

[5] Fleischer, O. (2014) *Axial beanspruchte K-Knoten aus dünnwandigen Rechteckhohlprofilen* [Dissertation]. Karlsruher Institut für Technologie.

[6] Yao, Z.; Wilkinson, T. (2015) *Experimental investigation of the static capacity of grade C450 RHS K and N truss joints* in: Batista; Vellasco; Lima [eds.] *Tubular Structures XV, Proceedings of 15th Symposium of Tubular Structures, Rio de Janeiro, Brasil*.

[7] Tuominen, N.; Björk, T. (2017) *Capacity of RHS-Joints made of high strength steels*. CIDECT Report 5BZ.

[8] Björk, T.; Saastamoinen, H. *Capacity of CFRHS X-joints made of double-grade S420 steel*. Tubular Structures XIV, pp. 167–176.

[9] Becque, J.; Wilkinson, T. (2017) *The capacity of grade C450 cold-formed rectangular hollow section T and × connections: An experimental investigation*. Journal of Constructional Steel Research 133, pp. 345–359. https://doi.org/10.1016/j.jcsr.2017.02.032

[10] prEN 1993-1-8:2021-03 (2021) *Eurocode 3: Bemessung und Konstruktion von Stahlbauten – Teil 1-8: Bemessung von Anschlüssen; Deutsche und Englische Fassung prEN 1993-1-8:2021*. Berlin: Beuth Verlag GmbH.

[11] Lan, X.; Chan, T.-M.; Young, B. (2017) *Static strength of high strength steel CHS X-joints under axial compression*. Journal of Constructional Steel Research 138, pp. 369–379. https://doi.org/10.1016/j.jcsr.2017.07.003

[12] DIN EN 10219-3:2020-11 (2020) *Kaltgeformte geschweißte Hohlprofile für den Stahlbau – Teil 3: Technische Lieferbedingungen für höher- und wetterfeste Stähle; Deutsche Fassung EN 10219-3:2020*. Berlin: Beuth Verlag GmbH.

[13] DIN EN 10210-3:2020-11 (2020) *Warmgefertigte Hohlprofile für den Stahlbau – Teil 3: Technische Lieferbedingungen für höher- und wetterfeste Stähle; Deutsche Fassung EN 10210-3:2020*. Berlin: Beuth Verlag GmbH.

[14] Ummenhofer, T.; Kuhlmann, U.; Engelhardt, I.; Feldmann, M. et al. (2022) *Statische Tragfähigkeit von geschweißten, hochfesten Hohlprofilknoten – FOSTA Forschungsverbund HOCHFEST: Projekte "Hochfeste Hohlprofilknoten"*, Stahlbau 91, No. 10, pp. 633–646. https://doi.org/10.1002/stab.202200056

[15] DIN EN 10204:2005-01 (2005) *Metallische Erzeugnisse – Arten von Prüfbescheinigungen; Deutsche Fassung EN 10204:2004*. Berlin: Beuth Verlag GmbH.

[16] DIN EN 1090-2:2024-09 (2024) *Ausführung von Stahltragwerken und Aluminiumtragwerken – Teil 2: Technische Regeln für die Ausführung von Stahltragwerken; Deutsche Fassung EN 1090-2:2018+A1:2024*. Berlin: Beuth Verlag GmbH.

[17] Lu, L. H.; Winkel, G. D.; Yu, Y.; Wardenier, J. (1994) *Deformation limit for the ultimate strength of hollow section joints* in: Grundy, P.; Holgate, A.; Wong, B. (eds.) *Tubular structures VI: Proceedings of the 6th international symposium on tubular structures*. Melbourne, Australia: Routledge.

[18] Zhao, X.-L. (2000) *Deformation limit and ultimate strength of welded T-joints in cold-formed RHS sections*. Journal of Constructional Steel Research 53, No. 2, pp. 149–165. https://doi.org/10.1016/S0143-974X(99)00063-2

[19] DIN EN 1990:2021-10 (2021) *Eurocode: Grundlagen der Tragwerksplanung; Deutsche Fassung EN 1990:2002_+ A1:2005_+ A1:2005/AC:2010*. Berlin: Beuth Verlag GmbH.

Authors

Adrian Münch, M.Sc. (corresponding author)
adrian.muench@kit.edu
Karlsruhe Institute of Technology
KIT Steel and Lightweight Structures
Otto-Ammann-Platz 1
76131 Karlsruhe
Germany

Dr.-Ing. Philipp Weidner
philipp.weidner@kit.edu
Karlsruhe Institute of Technology
KIT Steel and Lightweight Structures
Otto-Ammann-Platz 1
76131 Karlsruhe
Germany

Prof. Dr.-Ing. Thomas Ummenhofer
thomas.ummenhofer@kit.edu
Karlsruhe Institute of Technology
KIT Steel and Lightweight Structures
Otto-Ammann-Platz 1
76131 Karlsruhe
Germany

Valentin Larasser, M. Eng.
valentin.larasser0@hm.edu
Institut für Material und Bauforschung
Hochschule München
Karlstr. 6
80333 München
Germany

Pauline Markreiter, M. Eng.
pauline.markreiter@hm.edu
Institut für Material und Bauforschung
Hochschule München
Karlstr. 6
80333 München
Germany

Prof. Dr.-Ing. Imke Engelhardt
imke.engelhardt@hm.edu
Institut für Material und Bauforschung
Hochschule München
Karlstr. 6
80333 München
Germany

How to Cite this Paper
Münch, A.; Weidner, P.; Ummenhofer, T.; Larasser, V.; Markreiter, P.; Engelhardt, I. (2025) *Experimental investigations of T-joints made of high-strength square hollow sections*. Steel Construction 18, No. 3, pp. 180–193. https://doi.org/10.1002/stco.202500026

This paper has been peer reviewed. Submitted: 24. June 2025; accepted: 10. July 2025.